MODELLING OF THE PERMEABILITY OF A WEAKLY CONSOLIDATED OTTER SHERWOOD SANDSTONE UNDER PROPORTIONAL TRIAXIAL COMPRESSION STRESS PATHS

Nguyen Van Hung, Le Phuoc Hao
Petrovietnam University
Email: hungnv@pvu.edu.vn

Summary

Laboratory experiments under hydrostatic and triaxial stress path (ratio of increasing both vertical and horizontal stress) testing have been performed on three materials: clean unconsolidated quartz sand (coarse grains or angular), fine to medium grained weakly cemented layered sandstone, the Otter Sherwood sandstone, and outcrop analog of the Sherwood reservoir of the Wytch Farm oil field (UK). The elastic and plastic deformation regimes are well identified and the determined yield stresses are fitted using the modified Cam-clay and Elliptic Cap models for all the observed onsets of plastic yielding [1]. Both vertical and horizontal permeability have been measured during loading. Geometric factor was determined by using numerical simulation and/or measurement in the laboratory in order to calculate the horizontal permeability. The permeability can be closely controlled by the mean pressure and/or deviatoric stress and can be clearly observed by the isopermemability-stresses diagrams. Finally, one application of elastic-plastic to prediction of the behaviour of material is presented. The prediction of the directional permeability evolution with stresses is then obtained using an exponential equation of an effective strain.

Key words: *Geomechanics, stress paths, Wytch Farm, Otter Sherwood sandstone, weakly consolidated, permeability.*

1. Introduction

During hydrocarbon production, the decrease of pore pressure (depletion) induces anisotropic effective stress increases, which depend on the reservoir rock properties, leading to the compaction of the reservoir. In the worst case, inelastic deformations and irreversible reduction of porosity may induce subsidence issues in the oil fields with severe consequences such as well failure, permeability reduction, and reservoir impairment [2]. Unconsolidated or weakly consolidated reservoir rocks with high porosity and low cohesive strength are prone to experience large strains as well as drastic decrease of permeability under stress. The predictions of strain and permeability evolutions are important objectives of reservoir engineering, in order to control and optimise hydrocarbon recovery. Thus, it is important to have a fundamental understanding of the compaction mechanisms and its effect on anisotropy permeability development.

In previous studies on the depletion-induced reservoir compaction, laboratory experiments mimic in-situ stress paths by performing either uniaxial deformation tests (oedometric case: only vertical compaction without horizontal deformation) [3] or hydrostatic tests [4], easier to handle in the laboratory. Between the uniaxial strain technique and hydrostatic stress test, they realised hydrostatic stress test because it is easier to conduct in the laboratory. Then the one-dimensional pore volume (formation) compressibility "C_f" is calculated by Eq. (1) from pore compressibility "C_p" derived from hydrostatic testing [4]:

$$C_f = C_p * USCP_{e(p)} \quad (1)$$

Where $USCF_e$ represents the elastic uniaxial strains correction factor for small strain and $USCF_p$ represents the plastic uniaxial strain correction factors for large strain, they can be determined in Eq. (2) and Eq. (3):

$$USCF_e = \frac{1+\nu}{3(1-\nu)} \quad (2)$$

$$USCF_p = \frac{1+2k_0}{3} \quad (3)$$

Where "ν" is a constant Poisson's ratio, and "k_o" is termed the "coefficient of earth pressure at rest".

Yet, hydrostatic state of stress is rarely found in-situ in produced reservoirs; it would imply a similar evolution of vertical and horizontal effective stresses during production. Segura et al. [5] suggest that stress arching effects can prevent the overburden weight to be transmitted to the side burden during reservoir compaction. Furthermore, for the uniaxial deformation case, the boundary conditions consider only high aspect ratio reservoirs (i.e. vertical thickness<<lateral extent). Ruistuen et al. [6] explained that the exact nature of the boundary conditions in reservoirs is uncertain, and the uniaxial strain condition may thus not be appropriate in all cases. These boundary conditions depend on several parameters: size and geometry of the reservoir, contrasts

in poroelastic properties between the reservoir rock and surrounding formations, and their inelastic deformations.

To go further and get flexibility in simulating the in-situ stress changes during the production, Rhett and Teufel [7] proposed the definition of the stress path parameter $K=\Delta\sigma'_h/\Delta\sigma'_v$ defined as the ratio of the change in effective horizontal stress by the change in effective overburden stress from initial reservoir conditions. With this definition, hydrostatic loading corresponds to K = 1, whereas a "classical" triaxial test with constant confining pressure corresponds to K = 0. For example Rhett and Teufel [7] found from in situ measurements in the Ekofisk Field a value K ~ 0.2 for the stress path parameter during production. However from laboratory uniaxial strain tests, they measured K ranging between 0.4 and 0.6, depending on the rock type. Thus, the stress path parameter K can not be obtained only from the rock properties but must be compared to in situ stress measurements. Reservoir engineers usually use the relationship $K = \nu/(1-\nu)$ to relate the elastic behaviour and the stress path K (sometimes called "K_o") which can be obtained from uniaxial strain tests [6, 8]. Many studies have been trying to explain the results obtained in the laboratory and fit all results under different stress path K by using the theory. Eq. (4) presented one relationship linearly of increased stress anisotropy ($\Delta Q = \Delta\sigma'_v - \Delta\sigma'_h$) while the pressure drop increases ΔP_p:

$$\Delta Q = -\alpha (1 - K)\Delta P_p \quad (4)$$

Several studies have demonstrated that the compaction behaviour of siliciclastic and carbonate rocks presents similar macroscopic features at low temperature [9, 10] but also highlights different micromechanisms of damage at the microstructure scale. The inelastic compaction is often associated with grain crushing and pore collapse. The grain crushing pressure can be predicted by the model proposed by Zhang et al. [11] for siliciclastic rocks based on the Hertzian fracture model, or by a pore-emanated cracking model in carbonate rocks [12]. Once the pressure reaches the yield point, the plastic strains are accommodated either through brittle fracture or pore collapse, resulting in moderate changes to drastic permeability reduction.

From the hydromechanical point of view, numerous authors, e.g [6, 7, 13, 14, 15], have explored the impact of the stress path on the compaction and on the vertical permeability (k_v) (parallel to the maximum stress direction) evolution in different analog and reservoir sandstones. Generally, they measured a permeability reduction as the stress path becomes more deviatoric.

Very few studies are reported in the literature on the horizontal permeability k_h measurements (perpendicular to the maximum stress direction). Zhu et al. [16] measured the anisotropy of permeability with classical axial flow using triaxial extension tests and "hybrid" (proportional) compression tests. Another method was used by Crawford et al. [17] and Dautriat et al. [18]: they measured the anisotropy of permeability by non-conventional transverse radial flows under triaxial and proportional compression tests, requiring to correct Darcy's law using a geometrical factor accounting for the complex geometry of the radial flow [19].

Another problem needs also to be addressed when permeability measurements are concerned, the hydromechanical end-effects which can alter the measurements by increasing the pressure drop [18, 20, 21].

Once the permeability data are available from either laboratory or/and *in situ* tests, the productivity index PI representing the ability of a reservoir to deliver fluids to the wellbore can be determined [22, 23].

To model the hydromechanical behaviour obtained in the laboratory under different stress paths K, Crawford et al. [24] used a "modified Cam-clay" elastoplastic model (symmetric ellipse) to fit the data obtained on unconsolidated sands compacted under different stress paths, extended to account for the evolution of permeability with deformation [25]. They add one parameter called "flattening" of the yield locus to modify an ellipse eccentricity. The elasto-plastic moduli (Young's modulus E, Poisson's ratio ν, hardening parameter λ and plastic potential g) can be calibrated by experiments as described by [25, 27, 28, 29] (Eq. (5)).

$$f = Q^2 + M^2 P'(P' - P_{co}) \quad (5)$$

Q: Deviatoric stress, $\Delta\sigma'_v - \Delta\sigma'_h$

P': Mean effective stress, $\frac{\Delta\sigma'_v + 2\Delta\sigma'_h}{3}$

M: Physical property of the material, control the shape of ellipse, related to the Mohr-Coulomb friction angle, φ, $M = (6\sin\varphi)/(3 - \sin\varphi)$.

P_{co}: Consolidation pressure, control the size of ellipse, correspond physically to the "memory" of the material.

However, it is very important and it is not easy to determine these parameters and these elastic properties (Young's modulus E, and Poisson's ratio ν), and hardening

parameter (λ), also plastic potential (g). Furthermore, reservoir engineers usually use the relationship Eq. (6) between elastic behaviour and stress path K (sometimes noted "K_o") which can be known from uniaxial strain tests.

$$K = \frac{\nu}{1 - \nu} \quad (6)$$

In the present study, we focus on the hydromechanical behaviour of very weakly consolidated sandstone, the triassic Otter Sherwood sandstone; it corresponds to the same formation as the Sherwood reservoir produced at the Wytch Farm oil field in Dorset/UK, operated since the early 1980s by BP and recently by Perenco. After describing the selected material and the experimental setup used for combining rock mechanics and directional fluid flow measurements, we will present our sets of experimental data. The main purpose is to provide a comprehensive database to characterise the basic hydromechanical behaviour of this stress dependent rock type. We apply elasto-plastic modelling to reproduce the rock behaviour along various stress paths and we predict the directional stress-dependent permeability evolution using a simple exponential formulation depending on the effective strain.

2. Sandstone description

The rock selected is the weakly consolidated Otter Sherwood sandstone (referenced hereafter as OSS) classified as a feldspathic arenite [30]. This sandstone belongs to the family of triassic Sherwood Sandstone group [31, 32] age of 200 - 250 Ma years being one of the reservoir rock of the nearby Wytch Farm oilfield in Dorset, South-West England; the Sherwood reservoir top is found at 1,585m true vertical depth subsea [33, 34]. Cores have been sampled on outcrops at Ladram Bay nearby in Devon, (Figures 1 and 2). The samples were cored perpendicular (V) and parallel (H) to the apparent bedding on cliff and outcrops (Figure 2).

Thin-sections and scanning electron microscope (SEM) were prepared to observe the nature of the rock microstructure. In Figure 3a black colour and in Figure 3b blue coloured resin

Figure 1. *South England map with Triassic outcrops [Modified from 35]; Ladram Bay (Devon county) location with triassic sandstone cliffs is marked with a cross; Wytch Farm oil field area below Poole Harbour (Dorset county) is hatched*

(a)

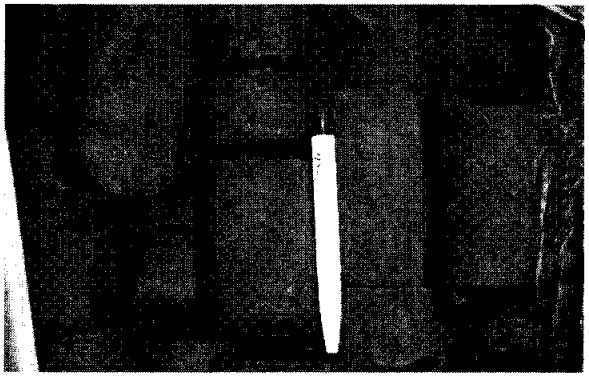

(b)

Figure 2. *Cliff with bedding at Ladram Bay, where the Otter Sherwood sandstone samples were cored (a); Core sample (b)*

(a)

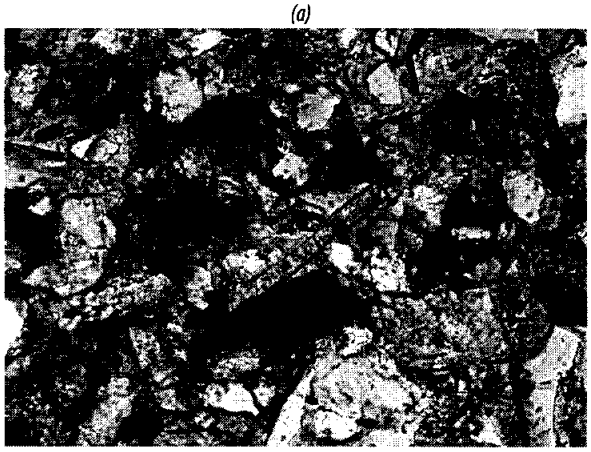

(b)

Figure 3. *Otter Sherwood sandstone SEM images (SE mode) (a); Vertical thin-section of Otter Sherwood sandstone (b)*

Table 1. *Mineralogical composition of the Otter Sherwood sandstone from [30]*

Mineralogy	Percentage (%)
Quartz	26.5 to 43.5
Feldspar	13 to 26
Clay (dominant Illite)	3.5 to 29
Mica	up to 7
Minor minerals	less than 3

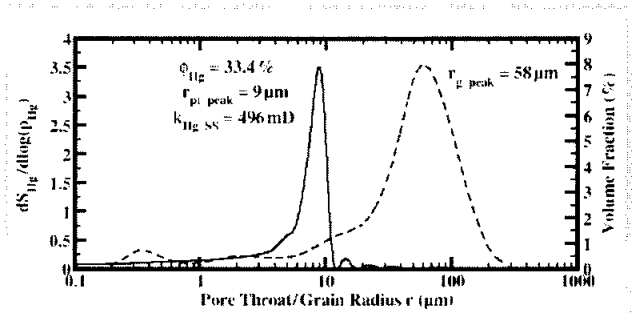

(a)

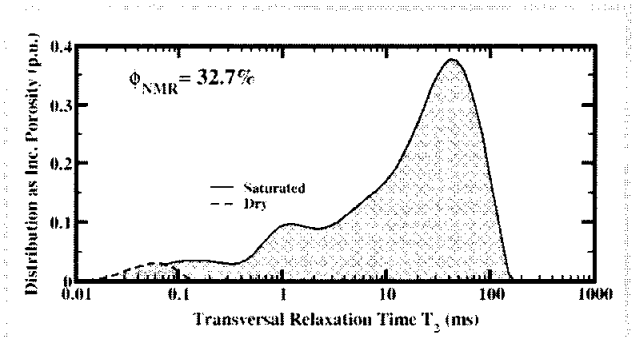

(b)

Figure 4. *"Qualitative" grain radius distribution of OSS by Laser Diffraction Granulometry, based on dominant mineral Quartz refractive index (peak at 58µm), pore-throat radius distribution (peak at 9 µm and tail down to 0.01µm) (a). NMR T2 relaxation time distribution of dry and saturated OSS samples (b)*

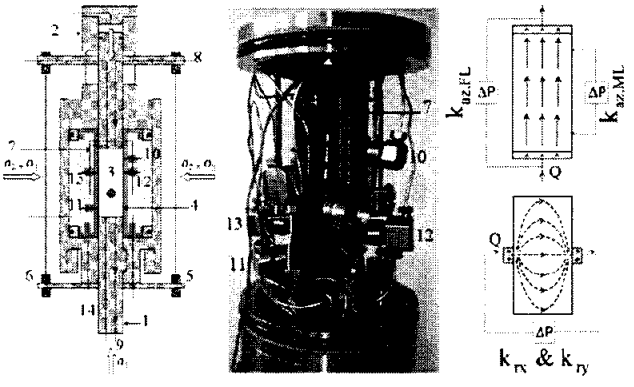

(a) *(b)* *(c)*

(1) fixed piston, (2) mobile piston, (3) sample, (4) sleeve, (5, 6) external LVDT, (7) internal cantilever, (8, 9) axial flow lines, (10, 11) pore fluid pressure samplers, (12, 13) radial flow ports, (14) external flow lines connectors

Figure 5. *Simplified sketch of the triaxial cell (a), picture of the equipped core sleeve (b), pressure differential and flow configurations for permeabilities kaz,FL, kaz,ML and krxy (c)*

highlight high porous layers of detrital angular quartz grains separated by fine grained laminations.

The mineralogical composition of OSS has been described by Svendsen and Hartley [30] and is detailed in Table 1. Thin sections analysis (Figure 3a) confirms this mineralogical content.

The grain size distribution (volume equivalent dimension) of geomaterial was characterised by Laser Diffraction Method (Horiba apparatus) (Figure 4a) using the refraction index of the major mineral (Quartz) and assuming that the analysed particles have an isotropic shape. The grain size spreads from 10 to 500µm, with a peak at 116µm. SEM observation on fresh surfaces (Figure 3) shows the major detrital grains (quartz and K-Feldspar) with sizes compatible with the LD measurement. In Figure 4a, the mercury injection curve reveals a narrow distribution of pore throats around 9µm. The porosity of OSS given by Hg porosimetry is 33.4%, and the one given by NMR measure is 32.7% (Figure 4b). Permeability estimation from Hg porosimetry (Swanson's sandstone correlation) is 496mD.

3. Equipment and procedures

3.1. Triaxial cell and measurements

The hydraulic triaxial cell used for this study is illustrated in Figure 5. The cell is operated with two high-pressure pumps (up to 69MPa) working independently to control the confining pressure and the axial load (up to 80kN) in order to test different stress paths. The pore pressure regulation is achieved by a back pressure system while the flow is generated by a lower pressure pump (up to 25MPa) [1, 18].

In order to measure the large vertical and radial displacement in weakly consolidated materials (up to

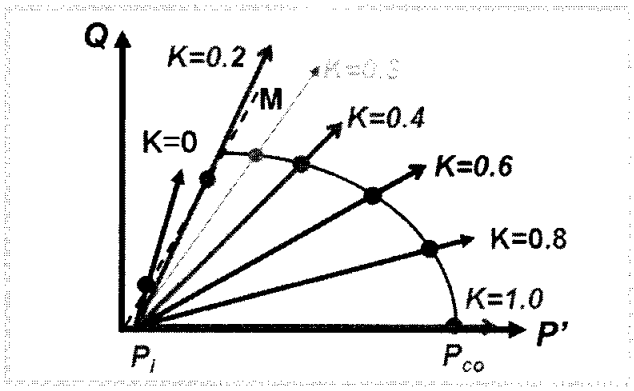

Figure 6. *Selected stress paths to characterise the hydro-mechanical behaviour of Otter Sherwood sandstone: triaxial (K = 0) and proportional triaxial (K > 0) compression tests.*

few mm), we used a couple of linear variable differential transducers (LVDT) and a dual cantilever sensor fastened to the core sleeve. The volumetric (ε_V) and deviatoric (ε_Q) strains are calculated from the measured axial (ε_a) and radial (ε_a) strains as respectively $\varepsilon_V = \varepsilon_a + 2\varepsilon_r$ and $\varepsilon_Q = 2(\varepsilon_a - \varepsilon_r)/3$ on the assumption of conservation of the cylindrical shape during loading [1].

The permeability can be measured in three orthogonal directions. In the axial direction (direction of maximal stress), the vertical permeability k_v is measured in two different ways, firstly on the total length of the sample (~80mm), secondly at an intermediate distance (60mm) corresponding to the spacing of two local pressure ports located radially on the sleeve. The horizontal permeability k_h is measured in two orthogonal radial directions in the lower and upper parts of the sample across two diameters. The determination of the geometrical factor G, is required to correct Darcy's law to obtain the true radial permeability [17 - 20]. To monitor the pore pressure, the fluid pressure is also measured at the bottom of the sample near the flow inlet.

***Table 2.** Summary of the experimental parameters and petrophysical characterisation of the four samples sets*

Sample Vertic/ Horizont Dry/Wet	Stress Path K	Porosity (%)	Overall Axial Perm. (mD)	Mid. Axial Perm. (mD)	Ratio $k_{v,L}/k_{v,M}$
Set 1 (Wet Vertical Samples for k_v measurements)					
OSS_A V W	1.0	34.1	142	182	0.78
OSS_B V W	0.8	31.0	168	215	0.78
OSS_C V W	0.6	33.7	208	258	0.81
OSS_D V W	0.4	33.4	148	182	0.81
OSS_E V W	0.2	31.0	155	222	0.70
OSS_F V W	0	33.5	147	164	0.90
Set 2 (Wet vertical samples for k_h measurements)					
OSS_G V W	1.0	34.4	105	133	0.79
OSS_H V W	0.8	33.4	85	117	0.73
OSS_I V W	0.6	32.4	121	143	0.85
OSS_J V W	0.4	32.0	178	245	0.73
OSS_K V W	0.2	31.4	142	158	0.90
Set 3 (Wet Horizontal Samples for k_h measurements)					
OSS_M H W	1.0	33.0	276	350	0.79
Set 4 (Dry vertical sample)					
OSS_L V D	1.0	-	-	-	-

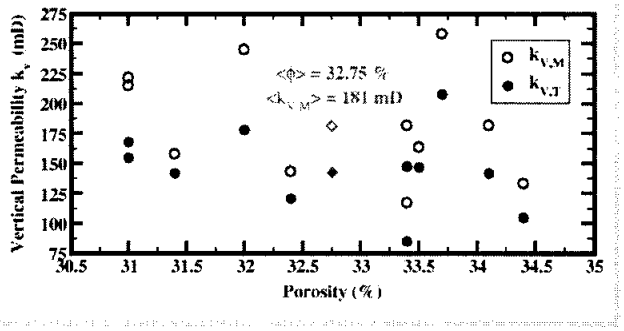

***Figure 7.** Crossplot of porosity and vertical permeability values for the 11 samples of sets 1 and 2 in Table 2; mean porosity is 32.75% and average vertical permeability is 181mD*

3.2. Compression test procedures

The stress path parameter K [7], defined in introduction, is related to h, the slope of the linear stress path in the (P', Q) stresses plane by the relationship: $\eta = 3(1-K)/(1+2K)$ (Figure 6); $P' = (\sigma'_a + 2P'_c)/3$ is the mean effective stress and $Q = \sigma' - P'_c$ is the deviatoric stress. Thus different stress paths K were investigated in this study, in order to fully characterise the hydromechanical behaviour of the OSS: (1) Drained hydrostatic compression K = 1, (2) Drained proportional triaxial stress paths with constant K = 0.8; K = 0.6; K = 0.4; K = 0.2 and (3) Drained classical triaxial stress path with K = 0 (constant confining pressure). A unique axial loading rate, $\dot{\sigma}_a$ =0.1MPa/min, was selected for all the tests which corresponds to axial strain rates $\dot{\varepsilon}_a$ of the order of 1×10^{-5} to $4 \times 10^{-7} s^{-1}$. The high permeability of OSS guarantees the drained condition.

4. Samples preparation

Two types of samples were cored parallel (H) and perpendicular (V) of bedding with the length of around 80 mm, diameter of around 38.1 mm. All samples were dried inside an oven at no more than 60°C for at least 48 hours until a constant weight is reached. The dry density profiles of each sample were measured using the X-ray-CT-Scanner and the porosity of each core has been estimated first in unconfined condition. We selected for the mechanical tests only the sample which looked homogeneous on the density maps.

In order to minimise, or even eliminate, possible reactions between the rock minerals and the fluid saturated, the proposed methodology suggests the use of a NaCl brine (at concentration $20g.L^{-1}$). This brine was verified that it cannot damage the equipment. Laboratory regulated temparature of 20°C was sufficient to get a viscosity of 1 cp.

The samples initially in dry state were first loaded hydrostatically up to a pressure close to 2MPa to ensure sealing of the core sleeve on the sample and good setting of the radial extensometer. Initial deformations were measured and references were set. After minimal 3 hours of vacuum, the samples were saturated while

the pore pressure was regulated at 0.5MPa and hence pore volume and porosity were obtained (Table 2); NaCl brine at concentration 20g.L^{-1} was used as saturating fluid. Then using a small flow rate, about 3 pore volumes were circulated during one night to insure a good saturation by flushing residual trapped gas bubbles. Both measurements of initial vertical permeability were then determined simultaneously using the steady state flow method with flow rates ranging from 0.2 to 2cc/min. Laboratory temperature regulation of 20°C insures constant fluid viscosity and stable pressure drops during testing. For the set of H samples, the measurement of initial horizontal permeability was performed in the same way. The initial petrophysical properties of the samples are reported in Table 2. Figure 7 shows that there is no correlation between porosity and permeability at the scale of the OSS samples.

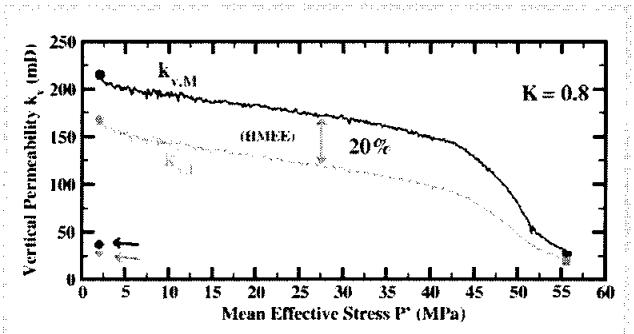

(a)

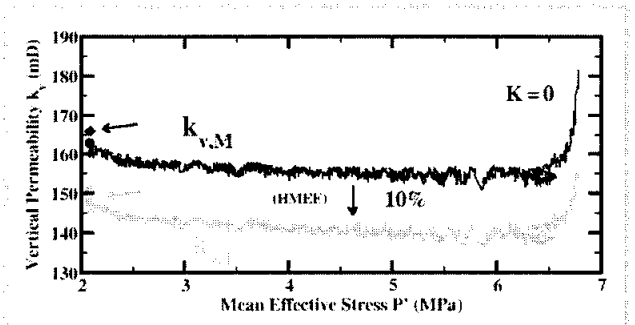

(b)

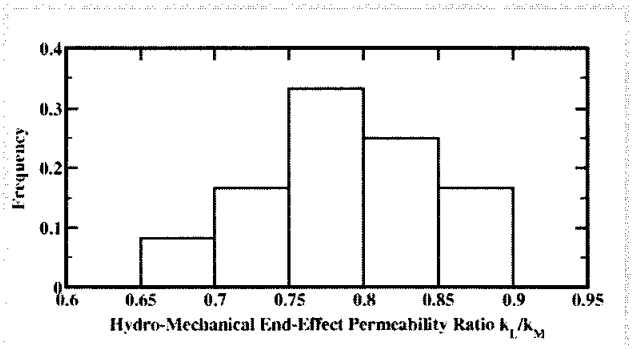

(c)

Figure 8. *Examples of hydro-mechanical end effects on vertical permeability measurements: intermediate measurements, unaffected by HMEE, show 10% to 30% of permeability gain compared to classical measurements (a, b); histogram of HMEE for the 11 samples of sets 1 and 2 (c)*

5. Permeability data

The vertical and horizontal permeabilities were measured using the continuous flow method during compaction under the different stress paths. Setting a single constant flow rate, the pressure drops were measured continuously during the loading in order to measure the permeability evolutions. Additionally, steady state measurements using different flow rates (higher accuracy) were performed at some stress reference levels (initial pressure, maximum stress at high K when the rate of plastic deformation is low, after unloading back to initial pressure) as quality control (see solid symbols in Figure 8); the difference between both kinds of measurements is about 3%, which is reasonable. Performing classical pressure step-wise measurements is in practice (1) time consuming and (2) prone to experimental problems when switching repeatedly between different flows lines network for directional permeability measurements. However, by operating in continuous mode, we were not able to measure anisotropic permeability development on a single sample, and we needed two sets of samples (V) and (H) to measure vertical and horizontal permeability separately.

5.1. Hydro-mechanical end effects

It has been shown in previous works [18, 20] that one has to worry about hydro-mechanical end effects (HMEE) when measuring permeability in the axial direction on core samples under stress. To illustrate this point we have plotted in Figure 8 the evolution of vertical permeability measured simultaneously on the full-length ($k_{v,L}$) and on the mid-length ($k_{v,M}$) for two stress paths.

In both cases the permeability is obtained from Darcy's law with the assumption that the entire core cross sectional area contributes to the flow. We observe that the mid-length permeability is systematically higher than the full-length permeability (Figure 8) in the range 10% to 20%. Such discrepancy has also been observed by Dautriat et al. [18, 20] on Fontainebleau and Bentheimer sandstones (up to 5% and 50%) and on Estaillades Limestone (up to 15%), and by Korsnes et al. [21] on Aalborg chalk (from 4% to 30%). This effect is attributed to hydromechanical end-effect in the vicinity of the rock/piston interface: it is significant and should be taken into

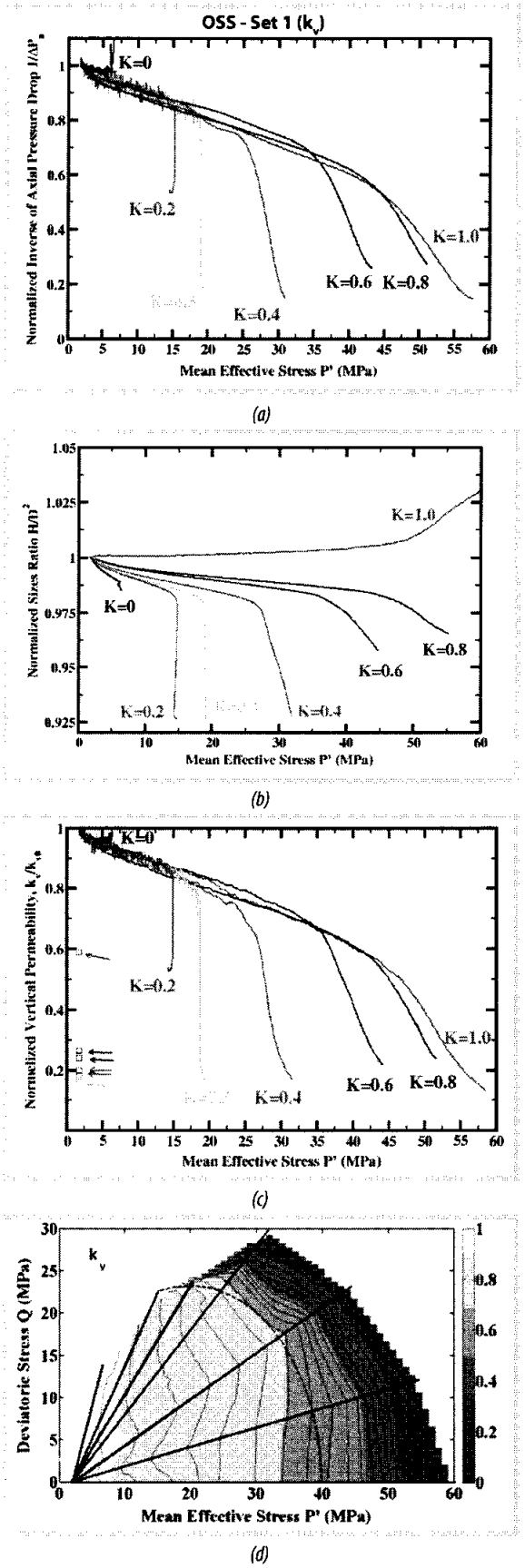

Figure 9. *Stress path dependent: normalised intermediate pressure drops evolutions (a); normalised ratio evolutions H/D^2 (b); normalised vertical permeability evolution (c) and normalised iso-vertical permeabilities in the (P' - Q) stress space (d).*

account in all studies involving permeability measurements. Despite the discrepancy in absolute values, we observe that the evolutions of both permeabilities with stresses are in fact comparable whatever the stress-path, meaning that stress dependent permeability evolution measured classically on the full length should still hold on similar weakly consolidated materials.

We cannot measure HMEE for horizontal permeability measurements, but they surely exist as well. On the one hand, as the injection zone is small, the local stress impact might be more pronounced, but on the other hand with this setup, we measure pressures as close as possible to the rock and expect to limit this effect [20].

5.2. Stress dependent vertical permeability

Despite CT-scan selection, the OSS samples show some scattering of initial vertical permeability measurements (spreading from ~150mD to ~250mD) due to microstructure heterogeneities. Figure 9 shows the results for normalised pressure drops and bulk deformation effect and for permeability evolutions with stress paths.

We observe that the axial pressure drop (Figure 9a) and the vertical permeability evolutions (Figure 9c) follow very closely the volumetric deformation evolutions ([1]); in fact, the permeability is controlled mainly by the pressure drop (term 1/DP in Darcy's law (Figure 9a)), i.e, by the viscous dissipation increase at pore throats levels (local deformations) and only slightly by the bulk deformations (term H/D^2 in Darcy's law (Figure 13b)) corresponding mainly to pores deformation. In the elastic deformation regime, for all stress paths except K = 0, the compression induces an important permeability reduction associated with compaction varying between 30% and 40% as K decreases towards 0.2. Then in the plastic deformation regime, the permeability decreases more and more rapidly as K becomes smaller.

As seen on Figure 9c, there is only a slight permeability recovery upon unloading. As shown in previous studies, the applied stresses possibly induce damage of grains by cataclasis (high K) and breakage (low K), shrinkage of the pore throats and production of fines clogging the pore throats. Deviatoric stress paths in the shear-enhanced compaction regime increase the damage and the permeability drops. A complementary microstructural study using thin-sections and microtomography is in progress to get more insight into the micro-mechanisms of damage.

The normalised vertical permeability evolutions are plotted in the (P', Q) stresses space from which iso-permeability

contours (vertical permeability only) are calculated by interpolation of the experimental data (Figure 9d). This mapping of permeability clearly highlights the fact that the permeability evolution is mainly controlled by the mean effective stress for all stress paths (iso-curves nearly vertical) up to the onset of inelasticity regime where the deviatoric stress starts to influence the permeability reduction (concavity of iso-curves). The permeability reduction rate is firstly a function of mean effective stress and later a function of stress path parameter as well.

5.3. Stress dependent horizontal permeability

Horizontal permeabilities have been measured on the second set of vertical samples (Table 2). Figure 10 shows the results for the normalised pressure drops. The effect of deformation is small compared to radial pressure drop evolutions (same order as in Figure 9b) and the pressure drop as response of local deformations at pore throats level drives the horizontal permeability.

Compared to the axial measurements, the radial pressure drops are more important for all stress paths, except for K = 0.2. This could be either due to evolution of HMEE while loading (which was not observed for axial measurements) or to an evolution of initial anisotropy k_h/k_v with stress path.

5.3.1. Geometrical factor in isotropic case

Darcy's law needs to be corrected to calculate horizontal permeability k_h. Instead of a uniform flow section (radial injection area S_a), the radial flow shows diverging/converging stream lines (Figure 11b), interpreted as a true radial cross-sectional area of flow (S_n). For an isotropic porous rock, a geometrical factor G, defined in Eq. (7), is used to correct the Darcy's law (Eq. (8)) as proposed by [19]:

$$G = S_a/S_n \quad (7)$$

$$k_h = G.\frac{q}{S_a}\mu\frac{D}{\Delta P} \quad (8)$$

where k_h is the horizontal permeability, q is the volumetric flow rate, μ is the fluid viscosity, S_a is the cross sectional flow area, D is the sample diameter and DP is the pressure drop. G is a function of the set-up design (sample dimensions, flow ports dimensions and positions) and can be calculated by numerical simulations using Finite Elements Method as done by [17 - 20]. For our set up configuration, G = 0.1845.

During loading, the geometrical factor is dependent to some extent to the strains (ε_a, ε_r), as the dimensions

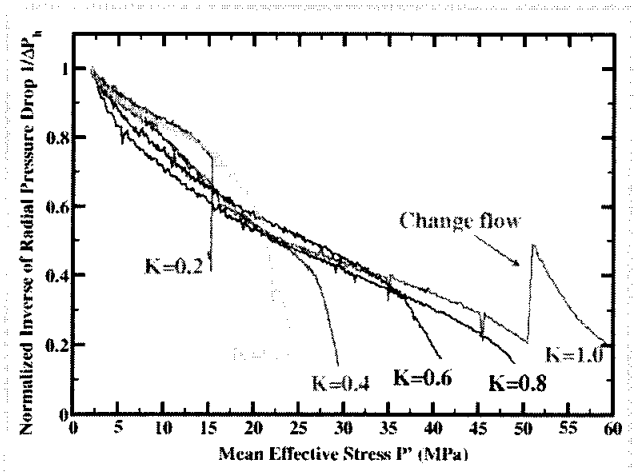

Figure 10. *Stress path dependent normalised pressure drop evolution for horizontal permeability measurements*

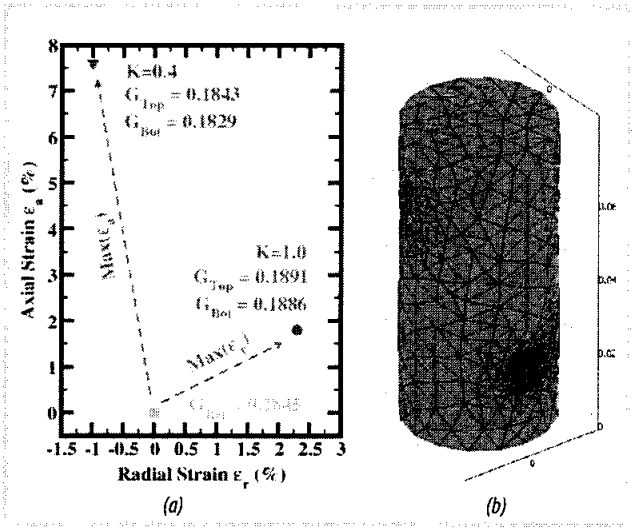

Figure 11. *Strain effects on the geometrical factor G for OSS, estimated using a F.E. modelling with the sample dimensions (80 mm of height, 38.1mm of diameter) and the sleeve geometry (9 mm of flow port diameter); (b) Radial flow simulation in a isotropic porous media showing radial flow.*

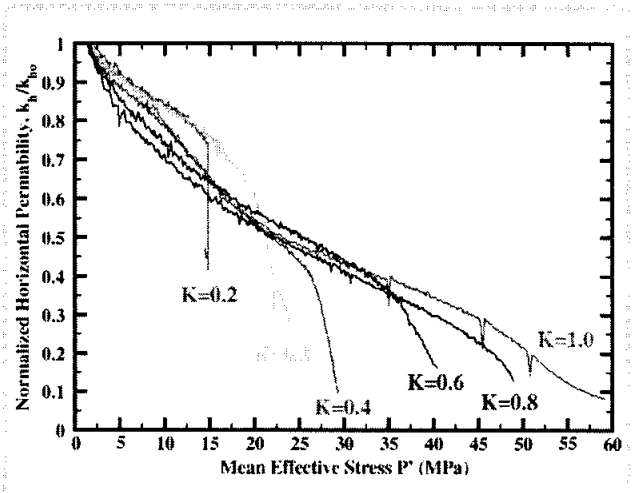

Figure 12. *Normalised horizontal permeability evolutions under the assumption of isotropy*

of the samples evolve [1]. We observe that under the different stress paths, the maximum strains are ε_a = +2%; ε_r = +0.75% in the elastic deformation regime and ε_a = 7%; ε_r = -1%/+2.7% in the plastic deformation regime. In agreement with Crawford et al., 2008 [17], this corresponds to small changes of G less than few %, as shown in Figure 11a.

Some authors have thus considered a constant geometric factor G, independent of strains, when studying the hydromechanical behaviour of stiff sandstones showing small deformations and none or small anisotropy or heterogeneous carbonates which anisotropy is difficult to define at the sample scale [18].

Under the assumption of isotropy, if we consider that G is independent of the strains in the range of applied stresses, the horizontal permeability can be calculated by Eq. (4). The normalised horizontal permeability evolutions are shown in Figure 12.

The horizontal permeability evolution for K = 0.8, K = 0.6, K = 0.4 are slightly similar and controlled by the mean effective stress up to the onset of inelasticity regime where the deviatoric stress starts to influence the permeability reduction. The permeability evolutions for K = 1.0 and K = 0.2 deviate from the 3 stress paths above. This might be due to the calculation method for horizontal permeability. It is possible that the assumption of isotropy leads to erroneous horizontal permeability evolution. In order to confirm this feature, it is necessary to consider the anisotropic permeability evolution due to compaction.

5.3.2. Anisotropy factor in anisotropic case

As the Otter Sherwood sandstone shows microstructural laminations (Figures 2 and 3) and seems to present permeability anisotropy (see Set 3 in Table 2), a second correcting factor should be introduced in the Darcy's law to take into account the anisotropic nature of OSS:

$$k_h = A.G.\frac{q}{S_a}\mu\frac{D}{\Delta P} \quad (9)$$

with A being the anisotropy factor, a function of the ratio (k_h/k_v) which can be calculated by Finite Element simulations as well as shown in Figure 13:

The anisotropy factor A is strongly dependent on the permeability ratio and follows for our set-up configuration a logarithmic trend in the permeability ratio interval [0.1 - 10]:

$$A = 1 + 0.536\ log_{10}(k_h/k_v) \quad (10)$$

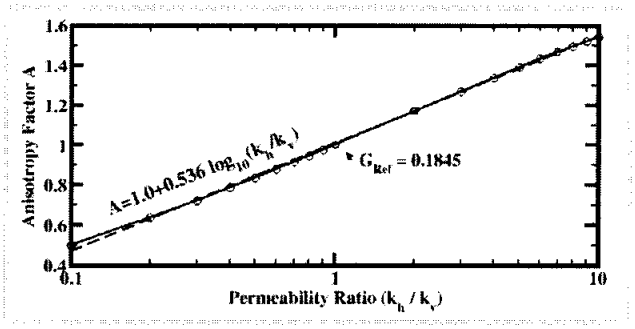

Figure 13. *Anisotropy factor evolution with permeability ratio*

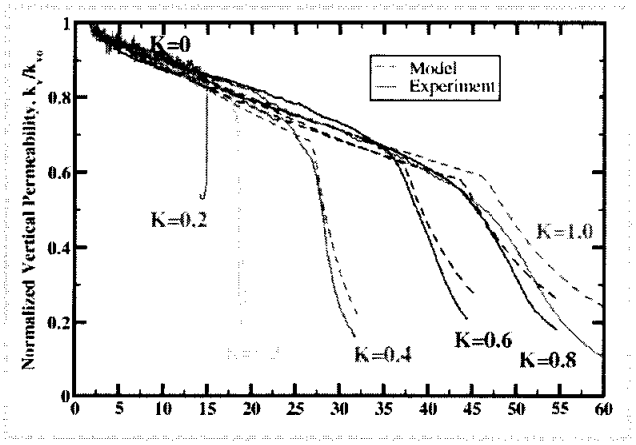

Figure 14. *Normalised vertical permeability evolutions with stress paths K, compared to experimental measurements*

While loading anisotropic rock, A is thus expected to evolve with k_h/k_v ratio; G can be considered as constant as the influence of strains is of second order compared to the anisotropy evolution.

However, as the evolution of the k_h/k_v ratio is *'a priori'* unknown, to calculate k_h, one needs either to proceed with an optimisation scheme or to solve the equation obtained by combining Eq. (9) and (10):

$$k_h - 0.536\ k_r.log_{10}\ k_h - k_r(1 - 0.536\ log_{10}\ k_v) = 0 \quad (11)$$

where $k_r = G.\frac{q}{S_a}\mu\frac{D}{\Delta P}$ is the radial apparent permeability, nothing else than (4), i.e. k_h calculated with the assumption of isotropy (A = 1). The solution of Eq. (11) can be obtained numerically or by using Lambert W function.

To calculate the horizontal permeability and its evolution with stress paths, we thus need to know k_v and its evolution with stress paths (Figure 9c). As we measured permeability continuously while loading and thus worked with two different sets of samples, we had to rely on the reasonable assumption that the normalised evolutions measured on the first set (Figure 9c) were also representative for the second set.

The horizontal permeability and permeability anisotropy evolutions inferred from this methodology will be presented in a future communication.

6. Hydromechanical modelling

We focus on the vertical permeability; to predict its evolutions, we use the formula proposed by Crawford et al. [25]:

$$k_v = k_{v0} exp(C.\varepsilon_{eff}), \quad (12)$$

where k_{v0} is the initial vertical permeability, C is a rock parameter fitted on our experimental data set (C = 0.22) and ε_{eff} is calculated from the effective strain increment $\delta\varepsilon_{eff} = \sqrt{\delta\varepsilon_V^2 + \delta\varepsilon_Q^2}$.

Figure 14 shows the predicted normalised vertical permeability versus mean effective stress compared to the data in Figure 9c.

Vertical permeability modelling is closer to the experimental data than the strain modelling. The concave part of permeability is modelled correctly. However, the elastic phase is not really linear like strain curves for all stress paths. It is evident that Eq. (8) is only used to model the permeability evolution when the shape of the yield cap is in concordance with the isopermeability contours, like Figure 9d. Indeed, when incremental plastic strain vectors are orthogonal (associated flow law) to the yield surface, these iso-permeability contours are also orthogonal to plastic strain increment vectors. In other situations, for triaxial measurements, if the permeability is controlled only by the mean effective stress P' and the reference effective stress P_0, we can use the formula $k = k_0.exp[-\gamma(P'-P_0)]$ proposed by David et al. [39].

7. Conclusions

The main results of this study on the hydromechanical behaviour of the weakly consolidated and laminated Triassic Otter Sherwood sandstone (outcrop analog for the Sherwood reservoir of the Wytch Farm oil field) can be summarised as follows:

- End effect may lead to erroneous measurement of absolute permeability values on the full length which is measured by classical method, but are not sensitive to compaction.

- Isopermeability contours in P':Q stress space are convex downwards and concordant with the shape of the yield cap.

- Porosity and permeabilities are unrecoverable under inelastic compaction: porosity decreases by few p.u. and permeabilities drop by one order of magnitude.

- Pore-throats tighten slightly and become clogged below 0.1μm. X-ray scanner resolution is not sufficient to characterise the damage process and localisation for stress paths K > 0.2; micro-structural analysis will help to link the mechanical and permeability evolutions.

- Vertical permeability can be modelised by combination of elasto-plastic and an exponential function of an effective strain. Smooth regime transition is not reproduced.

- Horizontal permeability measurement cannot be interpreted only by a 'geometry corrected Darcy's law'; as the permeability of the OSS is anisotropic, an anisotropy correcting factor is calculated and a procedure is proposed to calculate the evolutions of horizontal permeability with compaction.

References

1. Nguyen Van Hung, Le Phuoc Hao, Nicolas Gland. *Experimental study of hydromechanical behaviour of unconsolidated and weakly consolidated reservoir rocks.* Petrovietnam Journal. 2014; 10: p: 52 - 66.

2. M.Brignoli, Di Federico. *Compaction of unconsolidated sands and stress path effects: Laboratory evidence.* Proceedings of the 6th North America Rock Mechanics Symposium, Houston, Texas, US. 5 - 9 June, 2004.

3. G.H.Newman. *Pore-volume compressibility of consolidated, friable, and unconsolidated reservoir rocks under hydrostatic loading.* Journal of Petroleum Technology. 1973; 25(2): p.129 - 134.

4. B.R.Crawford, P.F.Sanz, B.Alramahi, N.L.DeDontney. *Modeling and prediction of formation compressibility and compactive pore collapse in siliciclastic reservoir rocks.* Proceedings of the 45th US Rock Mechanics/ Geomechanics Symposium, San Francisco, California, US. 26 - 29 June, 2011.

5. J.M.Segura, Q.J.Fisher, A.J.L.Crook, M.Dutko, J.G.Yu, S.Skachkov, D.A.Angus, J.P.Verdon, J.M.Kendall. *Reservoir stress path characterization and its implications for fluid-flow production simulations.* Petroleum Geoscience. 2011; 17(4): p. 335 - 344.

6. H.Ruistuen, L.W.Teufel, D.Rhett. *Influence of*

reservoir stress path on deformation and permeability of weakly cemented sandstone reservoirs. SPE Reservoir Evaluation & Engineering. 1999; 2(3): p. 266 - 272.

7. D.W.Rhett, L.W.Teufel. 1992. *Effect of reservoir stress path on compressibility and permeability of sandstones.* SPE Annual Technical Conference and Exhibition, Washington, US. 4 - 7 October, 1992.

8. C.T.Chang, M.D.Zoback. *Viscous rheology and state of stress in unconsolidated sands.* SPE/ISRM Rock Mechanics in Petroleum Enginering, Trondheim, Norway. 8 - 10 July, 1998.

9. Teng-fong Wong, Christan David, Wenlu Zhu. *The transition from brittle faulting to cataclastic flow in porous sandstone: Mechanical deformation.* Journal of Geophysical Research. 1997; 102(B2): p. 3009 - 3025.

10. P.Baud, S.Vinciguerra, C.David, A.Cavallo, E.Walker, T.Reuschlé. *Compaction and failure in high porosity carbonates: Mechanical data and microstructural observations.* Pure & Applied Geophysics. 2009; 166: p. 869 - 898.

11. Jiang Zhang, Teng-fong Wong, Daniel M.Davis. Micromechanics of pressure-induced grain crushing in porous rocks. Journal of Geophysical Research. 1990; 95(B1): p. 341 - 352.

12. Wei Zhu, Patrick Baud, Teng-fong Wong. *Micromechanics of cataclastic pore collapse in limestone.* Journal of Geophysical Research. 2010; 115(B4).

13. Rune M.Holt. *Permeability reduction induced by a nonhydrostatic stress field.* SPE Formation Evaluation. 1990; 5(4): p. 444 - 448.

14. F.M.R.Ferfera, J.P.Sarda, M.Boutéca, O.Vincké. *Experimental study of monophasic permeability changes under various stress paths.* International Journal of Rock Mechanics and Mining Sciences. 1997; 34(3/4): p. 37e1 - 37e12.

15. R.M. Ostermeier. *Compaction effects on porosity and permeability: Deepwater Gulf of Mexico turbidites.* Journal of Petroleum Technology. 2001; 53(2): p. 68 - 74.

16. Wenlu Zhu, Laurent G.J.Montési, Teng-fong Wong. *A probabilistic damage model of stress-induced permeability anisotropy during cataclastic flow.* Journal of Geophysical Research. 2007; 112(B10207): p. 1 - 22.

17. B.R.Crawford, D.W.Webb, K.H.Searles. *Plastic compaction and anisotropic permeability development in unconsolidated sands with implications for horizontal well performance.* Proceedings of the 42nd US Rock Mechanics Symsposium, San Francisco, US. 29 June - 2 July, 2008.

18. J.Dautriat, N.Gland, S.Youssef, E.Rosenberg, S.Bekri, O.Vizika. *Stress-dependent directional permeabilities of two analog reservoir rocks: A prospective study on contribution of μ-Tomography and pore network models.* SPE Reservoir Evaluation & Engineering. 2009; 12(2): p. 297 - 310.

19. M.Bai, F.Meng, S.Green. *Improved determination of stress-dependent permeability for anisotropic formations.* SPE/ISRM Rock Mechanics Conference, Irving, Texas, U.S. 20 - 23 October, 2002.

20. Jeremie Dautriat, Nicolas Gland, Jean. Guélard, Alexandre Dimanov, Jean L.Raphanel. *Axial and radial permeability evolution of compressed sandstones: End effects and shear-band induced permeability anisotropy.* Pure & Applied Geophysics. 2009; 166(5): p. 1037 - 1061.

21. R.I.Korsnes, R.Risnes, I.Faldaas, T.Norland. *End effects on stress dependent permeability measurements.* Tectonophysics 2006; 426(1 - 2): p.239 - 251.

22. S.D.Joshi. *Horizontal well technology.* PennWell Books. 1991.

23. Cosan Ayan, Nick Colley, Greig Cowan, Emmanuel Ezekwe, Mick Wannell, Peter Goode, Frank Halford, Jeffrey Joseph, Adriano Mongini, Julian Pop. *Measuring permeability anisotropy: The latest approach. Oilfield review.* 1994; 6(4): p. 24 - 35.

24. B.R.Crawford, M.J.Gooch, D.W.Webb. *Textural controls on constitutive behaviour in unconsolidated sands: Micromechanics and cap plasticity.* Proceedings of the 6th North America Rock Mechanics Symposium (NARMS), Houston, Texas. 5 - 9 June, 2004.

25. B.R.Crawford, D.W.Webb, K.H.Searles, G.Dasari, M.J.Gooch. *Plastic compaction and anisotropic permeability evolution in unconsolidated sand.* Communication at Euroconference of Rock Physics and Geomechanics, Oléron.

26. A.Schofield A. P.Wroth. *Critical state soil mechanics.* McGraw-hill. 1968.

27. D.M.Wood. *Soil behaviour and critical state soil mechanics.* 1st ed. Cambridge: University Press. 1990.

28. Ph.A.Charlez. *Rock mechanics: Volume 2 - Petroleum applications.* Edictions Technip. 1997.

29. R.Whitlow. *Basic soil mechanics (4th edition).* Prentice Hall. 2000.

30. J.B.Svendsen, N.R.Hartley. *Comparison between outcrop-spectral gamma ray logging and whole rock geochemistry: implications for quantitative reservoir characterisation in continental sequences.* Marine and Petroleum Geology. 2001; 18: p. 657 - 670.

31. S.Holloway, A.E.Milodowski, G.E.Strong, G.Warrington. The Sherwood sandstone group (Triassic) of the Wessex basin, Southern England. Proceedings of the Geologists' Association. 1989; 100(3): p. 383 - 394.

32. P.S.Spencer, K.P.Isaac. *Triassic vertebrates from the Otter sandstone formation of Devon, England.* Proceedings of the Geologists' Association. 1989; 94(3): p. 267 - 269.

33. A.J.C.Hogg, I.J.Evans, P.F.Harrison, T.Meling, G.S.Smith, S.D.Thompson, G.F.T.Watts. Reservoir management of the Wytch Farm oil field, Dorset, UK: Providing options for growth into later field life. Petroleum Geology Conference Series. 1999; 5: p. 1157 - 1172.

34. M.B.J.Bowman, N.M.Mcclure, D.W.Wilkinson. *Wytch Farm oifield: deterministic reservoir description of the Triassic Sherwood sandstone.* Proceedings of the Petroleum Geology of Northwest Europe. 1993: p. 1513 - 1517.

35. W.H.Mark, M.Gregg. *Magnetostratigraphy of the Sherwood Sandstone group (Lower and Middle Triassic), South Devon, UK: Detailed correlation of the marine and non-marine Anisian.* Palaeogeography, Palaeoclimatology, Palaeoecology. 2003; 193(2): p. 325 - 348.

36. P.Baud, W.Zhu, T-F.Wong. *Failure mode and weakening effect of water on sandstone.* Journal of Geophysical Research. 2000; 105(B7): p. 16371-16389.

37. M.D.Bolton. *The strength and dilatancy of sands.* Géotechnique. 1986; 36(1): p. 65 - 78.

38. D.P.Yale, B.Crawford, H.Watt. *Plasticity and permeability in carbonates: Dependence on stress path and porosity.* SPE/ISRM Rock Mechanics in Petroleum Engineering, Trondheim, Norway. 8 - 10 July, 1998.

39. Christian David, Teng-fong Wong, Wenlu Zhu, Jiaxiang Zhang. *Laboratory measurement of compaction-induced permeability change in porous rocks: Implication for the generation and maintenance of pore pressure excess in the crust. Pure & Applied Geophysics.* 1994; 143(1): p. 425 - 456.